



# The role of nanoparticles inclusion in monitoring the physical properties of PVDF

A. M. Ismail<sup>1</sup> · Rania Ramadan<sup>2</sup> · Mai M. El-Masry<sup>3</sup>

Received: 12 September 2022 / Revised: 8 December 2022 / Accepted: 26 December 2022 / Published online: 21 January 2023  
© The Author(s) 2023

## Abstract

In this work, the effects of  $\text{Co}_x\text{Zn}_{1-x}\text{Fe}_2\text{O}_4$  ( $x=0, 0.5, 1$ ) nanofillers on the PVDF polymer were scientifically studied. The structure and magnetic and optical properties were studied. XRD confirms the synthesis of nanofiller in a single phase. FTIR confirms the formation of nanoferrites. HRTEM shows that the prepared nanoferrites have a cubic-like shape. Also, the size and agglomeration increase with Co-Zn  $\text{Fe}_2\text{O}_4$  nanoferrites compared to the other singles one. The effect of adding nanoferrites into PVDF matrix was studied using XRD, FTIR, FESEM, VSM, and UV-Vis. XRD and FTIR approved the complexation between PVDF polymer and nanoferrites. Also, addition of nanoferrites into PVDF leads to decrease the semi-crystalline nature of PVDF. FESEM showed that embedding nanoferrites into PVDF polymers creates pores and PVDF/Co-Zn  $\text{Fe}_2\text{O}_4$  increases the pore size on the PVDF surface. The magnetic properties of PVDF were enhanced by adding the nanofiller. For example, saturation magnetization was increased from  $269.31\text{E}^{-6}$  to  $62.052\text{E}^{-3}$  by adding  $\text{CoFe}_2\text{O}_4$  to PVDF polymer. Band gap calculation showed that PVDF/Co-Zn  $\text{Fe}_2\text{O}_4$  has the lowest band gap energy which makes it useful in photochemical and electronic applications.

**Keywords** PVDF/nanoferrites · XRD · HRTEM · VSM · Optical properties · Electrical properties

## Introduction

Nanocomposite systems are now receiving the greatest interest from the scientific community due to their extensive use in a variety of applications, including sensors, microelectronics, photocatalysis, the biomedical field, and lithium-ion batteries [1–3]. In this direction, ferrite-based polymer nanocomposites are assumed as the highly effective one because of their unique characteristics, such as flexibility, low density, large surface area, low cost, and straightforward preparation methods [4].

The selection criteria of polymers and the nanofiller are very critical for adjusting the entire physical properties of the polymer-nanofiller matrix [5]. Poly vinylidene fluoride

(PVDF) polymer is a highly elastic and semi-crystalline material with significant ferroelectric and piezoelectric properties [6]. These properties make PVDF to be the most fascinating one in the polymer research field [7, 8].  $\beta$ -phase content is an important parameter and distinguishes the PVDF polymer which causes the ferroelectric properties of the PVDF polymer. Different types of organic and inorganic fillers were used to improve the  $\beta$ -phase content [9, 10].

Inclusion of magnetic nanoferrites such as  $\text{CoFe}_2\text{O}_4$  and  $\text{ZnFe}_2\text{O}_4$  as a filler in polymeric matrix can overcome the agglomeration limitation which is related to magnetic nanoferrites [7, 11]. On the other hand, nanoferrites which have high dielectric constants, such as  $\text{ZnFe}_2\text{O}_4$ , are appropriate for the design of several devices; however, due to the fragile nature of these ferrites, they have limited applications. Also, this drawback can be vanished by using PVDF as polymeric matrix for nanofiller [12–17]. The effects of magnetic fillers on the magnetic properties of PVDF polymer have been described by many studies. The antiferromagnetic character of PVDF loaded with various magnetic nanoparticles is confirmed by previously published research, and this behavior varies with temperature [18–20]. Additionally, as reported by Shandilya et al. [21], the same result may be obtained by

✉ Rania Ramadan  
rramadan@sci.cu.edu.eg

<sup>1</sup> Spectroscopy Department, National Research Centre, 33 El Bohouth Street, Dokki, Giza 12622, Egypt

<sup>2</sup> Materials Science Lab (1), Physics Department, Faculty of Science, Cairo University, Giza, Egypt

<sup>3</sup> Basic Science Dept., Higher Engineering Institute, Thebes Academy, Cairo, Egypt

using magnetic nanoparticles in several kinds of polymers such as ethyl cellulose, expanding the spectrum of uses for magnetic nanocomposites. The magnetic nanofillers had the advantages of improving the  $\beta$ -phase content and the magnetic properties of the polymer [9, 18–21].

Magnetic composites have a large specific surface area, strong hydrophilicity, and are often employed in many practical applications including photocatalysis, sensors, and chromatographic separation, and the current study is focused with the magnetic characteristics. Also, we are motivated to study the optical characteristics of the prepared samples because of the potential use of PVDF polymer in optoelectronic applications [22–24].

Moreover, we wanted to explore the impact of a composition with various ratios of  $\text{CoFe}_2\text{O}_4/\text{ZnFe}_2\text{O}_4$  on the characteristics of PVDF since many researchers examined PVDF filled with  $\text{CoFe}_2\text{O}_4$  and  $\text{ZnFe}_2\text{O}_4$ , which produces a noticeably improved performance of its features.

Herein, our aim is the fabrication of polymer nanocomposite films with approximately uniform distribution of the nanofillers which can help to improve many important properties. We expected that the inclusion of nanofiller with formula  $(\text{Co}_x\text{Zn}_{1-x}\text{Fe}_2\text{O}_4; x = 0, 0.5, 1)$  in PVDF matrix can improve its performance such as optical and magnetic properties. Even though this nanoferrite conducting PVDF polymeric matrix can provide new properties which differ than the individual counterpart properties, among the nanoferrite, this formula  $(\text{Co}_x\text{Zn}_{1-x}\text{Fe}_2\text{O}_4; x = 0, 0.5, 1)$  was chosen due to the thermal and chemical stability nature of Co-Zn ferrites which enables them to be used in memory and electronic devices.

## Methodology

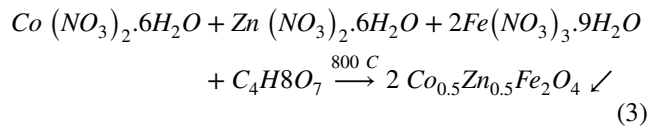
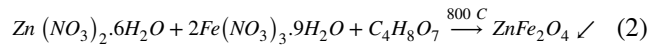
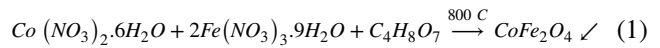
### Materials

Zinc nitrate [ $\text{Zn}(\text{NO}_3)_2 \cdot 6\text{H}_2\text{O}$ ], cobalt nitrate [ $\text{Co}(\text{NO}_3)_2 \cdot 6\text{H}_2\text{O}$ ], iron nitrate [ $\text{Fe}(\text{NO}_3)_3 \cdot 9\text{H}_2\text{O}$ ], PVDF [poly vinylidene fluoride] polymers, dimethyl sulphoxide (DMSO), and citric acid [ $\text{C}_6\text{H}_8\text{O}_7$ ] were purchased from LOBA, India.

### Preparation of nanoferrite

The citrate auto-combustion technique was used to produce nanosamples of  $(\text{Co}_x\text{Zn}_{1-x}\text{Fe}_2\text{O}_4; x = 0, 0.5, 1)$ . Powder phase (0.7 M) citrate acid thoroughly combined with (0.1 M) iron, zinc nitrates, and/or cobalt nitrates. The mixture's pH was then brought up to 7 through adjusting the ingredients. Finally, the mixture was heated to 250 °C until all traces of gas were gone, and the resulting powder was calcined at 800

°C for 2 h. Here are some equations that could be used to describe this process:



### Preparation of PVDF/nanoferrite nanocomposites films

For removing any moisture content, PVDF powder was dried at 60 °C in a vacuum oven for 2 h. Appropriate amount of PVDF (0.5 gm) was dissolved in dimethyl sulphoxide (DMSO) until entire solubility. Equal amounts (0.026 gm) of the prepared nanoferrite ( $\text{CoFe}_2\text{O}_4$ ,  $\text{ZnFe}_2\text{O}_4$ , and  $\text{Co}_{0.5}\text{Zn}_{0.5}\text{Fe}_2\text{O}_4$ ) was added to polymer solution forming three samples of PVDF/ $\text{CoFe}_2\text{O}_4$ , PVDF/ $\text{ZnFe}_2\text{O}_4$ , and PVDF/ $\text{Co}_{0.5}\text{Zn}_{0.5}\text{Fe}_2\text{O}_4$  to be (95/5 wt/wt.%). The nanocomposite mixtures were sonicated to avoid accumulation of nanoparticles, and then, the final solutions were transferred into Petri dish for 12 h at 60 °C.

### Measurement techniques

In order to perform an XRD study on the produced nanocomposites, a PANalyticalX'Pert Pro target Cu-K was used in conjunction with a secondary monochromator Holland radiation tube running at 45 kV and wavelength = 0.1540 nm. Data are collected using a VERTEX 80 FTIR spectrometer in the range 4000–400  $\text{cm}^{-1}$  (Bruker Corporation, Germany). The structure of the produced nanoferrites was seen by high-resolution transmission electron microscopy (HRTEM) utilizing a JEM-2100F electron microscope at 200 kV accelerating voltage. Quanta 250 FEG, run at 20–30 kV, was used for the FESEM analysis. A vibrating sample magnetometer (VSM) series of equipment was used for the magnetic measurements (Lake Shore VSM 7410). The Japanese-made Jasco UV-Vis (V-630) was used to acquire UV-Vis absorption spectra covering 190–1000 nm in wavelength.

## Results and discussion

### XRD

As shown in Fig. 1, the XRD pattern of nanopowder exhibits a spinel structure according to ICDD card no [01-089-8487]

**Fig. 1** XRD pattern of  $\text{Co}_x\text{Zn}_{1-x}\text{Fe}_2\text{O}_4$  and PVDF/ $\text{Co}_x\text{Zn}_{1-x}\text{Fe}_2\text{O}_4$  nanocomposite films ( $x = 0, 0.5, 1$ )

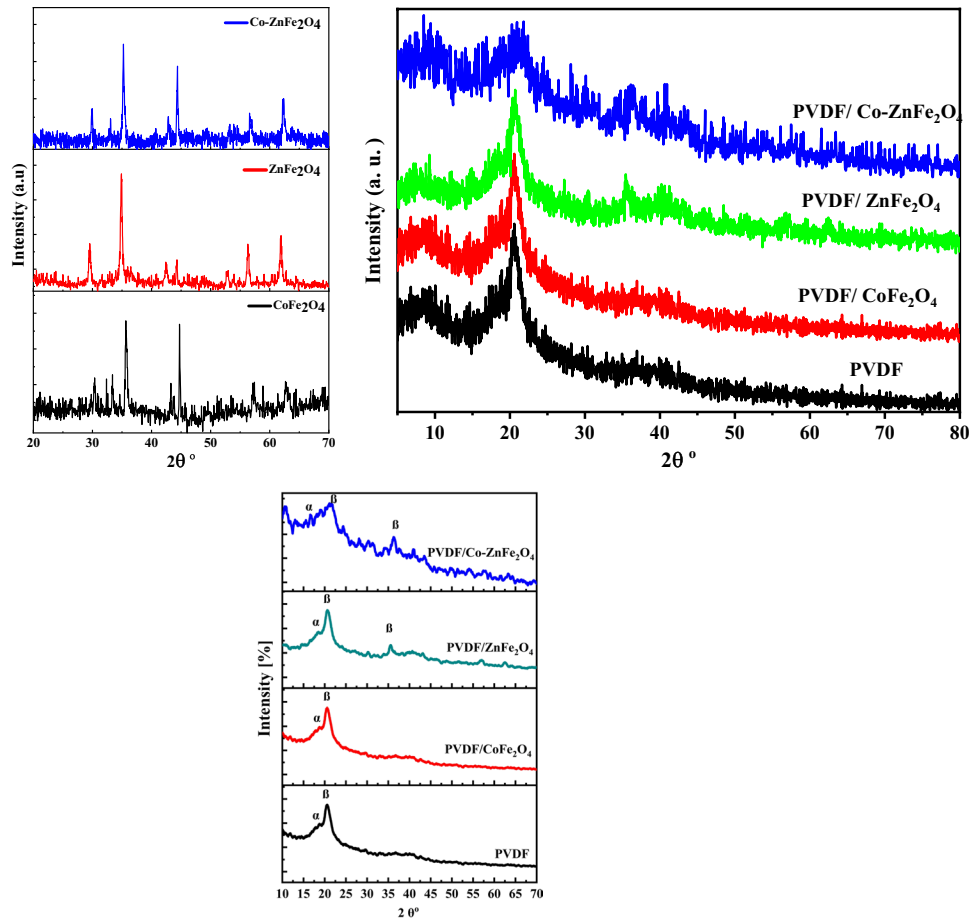


**Table 1** Crystallographic data of  $\text{Co}_x\text{Zn}_{1-x}\text{Fe}_2\text{O}_4$ ;  $x = 0, 0.5, 1$ , including crystallite size ( $D$ ), unit cell volume ( $V$ ), lattice parameters ( $a$ )

| Composition   | $D$ (nm) | $\text{CoFe}_2\text{O}_4$ |                       | $\text{ZnFe}_2\text{O}_4$ |                       |
|---|----------|---------------------------|-----------------------|---------------------------|-----------------------|
|   |          | $a$ (Å)                   | $V$ (Å <sup>3</sup> ) | $a$ (Å)                   | $V$ (Å <sup>3</sup> ) |
| $\text{CoFe}_2\text{O}_4$                             | 27       | 5.967                     | 212.45                |                           |                       |
| $\text{ZnFe}_2\text{O}_4$                             | 22       |                           |                       | 8.475                     | 608.67                |
| $\text{Co}_{0.5}\text{Zn}_{0.5}\text{Fe}_2\text{O}_4$ | 30       | 5.998                     | 215.78                | 8.461                     | 605.76                |

and [01-079-1150] related to  $\text{CoFe}_2\text{O}_4$  and  $\text{ZnFe}_2\text{O}_4$ , respectively. The average crystallite size of the prepared nanoferrites is calculated and listed in Table 1 by using Scherrer's equation [25]:

$$D = \frac{k\lambda}{\beta_{hkl} \cos \theta} \quad (4)$$

where  $D$  is the average crystallite size in nm,  $k$  is the shape factor (0.9), and  $\lambda$  represents the wavelength of the X-rays, while  $\beta_{hkl}$  related to the full width at half maximum (FWHM) expressed in radians, while  $\theta$  is the Bragg

diffraction angle. Based on the lattice parameters calculations, it was observed that, for the lattice parameter  $a$  related to Co-ferrite was 5.967 Å, it was increased to be 5.998 Å in the  $\text{Co-ZnFe}_2\text{O}_4$  composition. Even though the unit cell volume values were 212.45 (Å)<sup>3</sup> and 215.78 (Å)<sup>3</sup> for  $\text{Co}_2\text{FeO}_4$  and  $\text{Co}_{0.5}\text{Zn}_{0.5}\text{Fe}_2\text{O}_4$ , respectively, on the other hand, Zn-ferrite followed an opposite trend, as the lattice parameter  $a$  and unit cell volume were decreased from 8.475 Å and 608.67 (Å)<sup>3</sup> to 8.461 Å and 605.76 (Å)<sup>3</sup>, respectively, by the transition from Zn-ferrite to  $\text{Co}_{0.5}\text{Zn}_{0.5}\text{Fe}_2\text{O}_4$ .

Figure 1 displays the XRD of PVDF and PVDF/ $\text{Co}_x\text{Zn}_{1-x}\text{Fe}_2\text{O}_4$  ( $x = 0, 0.5, 1$ ) nanocomposite films. Pure PVDF shows a maximum semi-crystalline diffraction peak at  $2\theta = 20.5^\circ$  [26, 27]. It is observed that by addition of nanoferrites into PVDF polymers, the peak broadening increases and becomes more broadening for PVDF/ $\text{Co-ZnFe}_2\text{O}_4$ . Also, there is a noticeable decrease in the intensity of the diffraction peak at  $2\theta = 20.5^\circ$  PVDF/ $\text{Co-ZnFe}_2\text{O}_4$ , and it is shifted to higher 2 theta compared to the other doped nanoferrites. This approach confirmed that PVDF/ $\text{Co-ZnFe}_2\text{O}_4$  decreases the semi-crystalline nature of PVDF.

The (XRD) pattern indicates that the  $\beta$ -phase predominates, with small peak at  $18.30^\circ$  corresponding to the  $\alpha$ -phase. The sharp and intense peaks at  $19.85^\circ$  and  $35.90^\circ$  are due to the formation of the  $\beta$ -phase [28, 29].

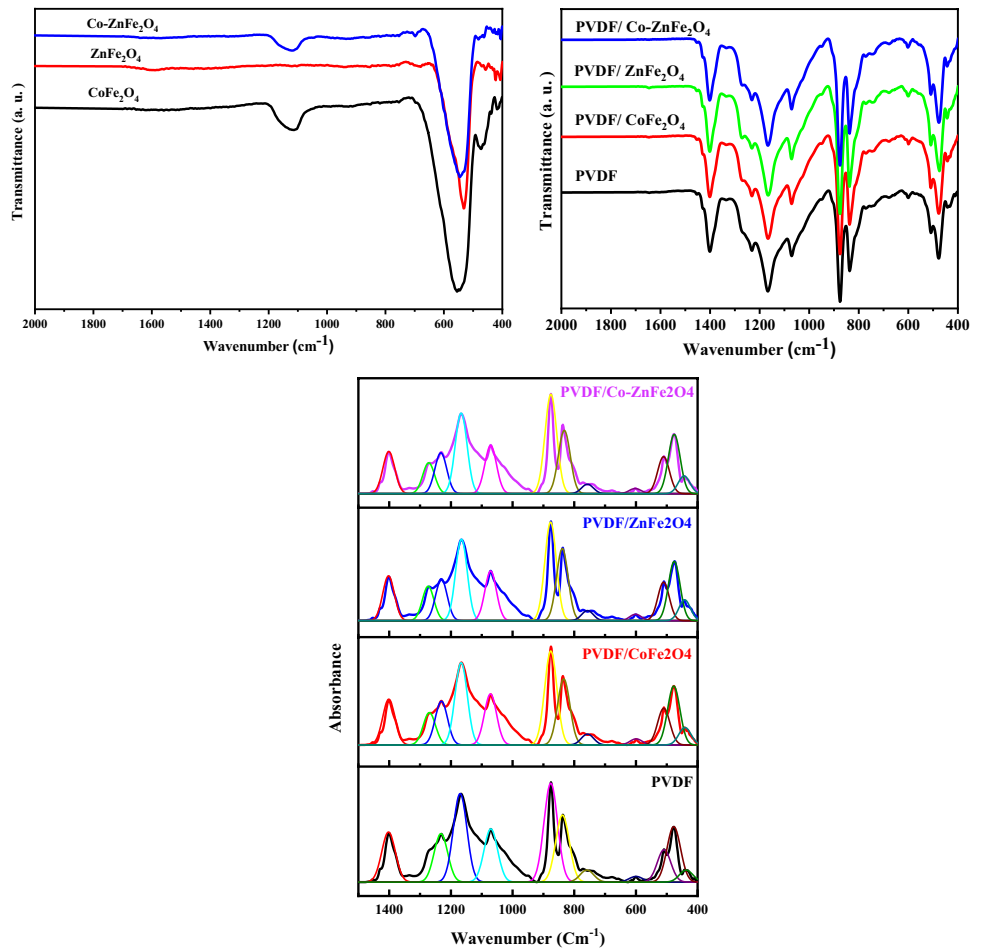
## FTIR

Figure 2 represents FTIR spectrum related to the prepared nanoferrites. Bands from  $600$  to  $500\text{ cm}^{-1}$  are related to the vibrational mode of  $M^{2+}-O^{2-}$  ( $M^{2+} = \text{Co}^{+2}$  and  $\text{Zn}^{+2}$ ) ( $\nu_1$ ) in the octahedral site). While bands between  $480$  and  $400\text{ cm}^{-1}$  describe the vibrational mode of  $\text{Fe}^{3+}-O^{2-}$  in the tetrahedral site [30–32], for  $\text{Co-ZnFe}_2\text{O}_4$ , it is observed that there are shifts in the bands compared to that in  $\text{CoFe}_2\text{O}_4$  and  $\text{ZnFe}_2\text{O}_4$ . The lengthening or shortening of bonds could account for this. The stretching mode energy responds to variations in unit cell volume via two mechanisms: shifts in bond length and shifts in the crystal field. When the unit cell is reduced and the crystal structure is brought closer together, for instance, the bond lengths typically contract, resulting in an increase in the stretching mode frequency. However, at the same time, the vibrating atoms feel a greater attraction to the adjacent ions, resulting in an increase in the dielectric constant of their local

surround and efficiently lowering the stretching frequency. However, increasing the average mass of the metallic ions participating in the stretch may account for the lower absorption frequencies achieved by exchanging the heavier Zn ion ( $M_w = 65.38\text{ g/mol}$ ) with the lighter Co ( $M_w = 58.93\text{ g/mol}$ ). Since the  $\nu_1$  band maximum increases during the transition from  $\text{CoFe}_2\text{O}_4$  to  $\text{Co}_{0.5}\text{Zn}_{0.5}\text{Fe}_2\text{O}_4$ , and decreases during the transition from  $\text{ZnFe}_2\text{O}_4$  to  $\text{Co}_{0.5}\text{Zn}_{0.5}\text{Fe}_2\text{O}_4$ , we may infer that the latter transition is responsible for the frequency changes.

The characteristic peaks for pure PVDF were observed at  $1401\text{ cm}^{-1}$  which is associated with  $\text{CH}_2$  wagging mode [33]. Two spectra bands at  $1167\text{ cm}^{-1}$  and  $1070\text{ cm}^{-1}$  were assigned for the asymmetric and symmetric stretching vibration of  $\text{CF}_2$ , respectively [34]. While  $\text{CF}_2$  bending vibration bands were recognized at  $601\text{ cm}^{-1}$  and  $477\text{ cm}^{-1}$  [35], the bending of C-H was observed at  $875\text{ cm}^{-1}$  [36]. There are two asymmetric stretching vibration bands that were related to C–C–C and C–F at  $837\text{ cm}^{-1}$  and  $772\text{ cm}^{-1}$ , respectively [37]. Bands at  $442\text{ cm}^{-1}$  and  $430\text{ cm}^{-1}$  are related to  $\text{CF}_2$  bending vibration. For PVDF/ $\text{Co}_x\text{Zn}_{1-x}\text{Fe}_2\text{O}_4$  nanocomposite films ( $x = 0, 0.5, 1$ ), the band at  $430\text{ cm}^{-1}$  is disappeared, and there is an increase in the intensity of the band at  $442\text{ cm}^{-1}$  which is associated

**Fig. 2** FTIR of  $\text{Co}_x\text{Zn}_{1-x}\text{Fe}_2\text{O}_4$  and PVDF/ $\text{Co}_x\text{Zn}_{1-x}\text{Fe}_2\text{O}_4$  nanocomposite films ( $x = 0, 0.5, 1$ )



with [metal $\leftrightarrow$ O] stretching vibration which approved the interaction between PVDF and the prepared nanoferrites.

We deconvoluted the FTIR spectra to calculate the relative percentage percent of  $\beta$ -phase in each sample in region from 1600 to 400  $\text{cm}^{-1}$ .

$F(\beta)$  is calculated using the following relation:

$$F(\beta) \% = \frac{A_{\beta}}{\frac{K_{\beta}}{K_{\alpha}} A_{\alpha} + A_{\beta}} \times 100 \quad (5)$$

where  $A_{\alpha}$  and  $A_{\beta}$  in Eq. (5) are the areas correspond to absorption peaks at 760  $\text{cm}^{-1}$  for  $\alpha$  and 840  $\text{cm}^{-1}$  for  $\beta$ -phases and  $K_{\alpha} = 6.1 \times 10^4$  and  $K_{\beta} = 7.7 \times 10^4 \text{ cm}^2/\text{mole}$  are the

absorption coefficients for  $\alpha$ - and  $\beta$ -phases. The bands at 444, 512, and 840  $\text{cm}^{-1}$  were regarded as characteristic of the  $\beta$ -phase. However, intensive absorption bands at 530, 614, and 796  $\text{cm}^{-1}$  are evidence of the high content of  $\alpha$ -phase [38].

Bands at 444, 512, and 840  $\text{cm}^{-1}$  were thought to be representative of the  $\beta$ -phase. Intense absorption bands at 530, 614, and 796  $\text{cm}^{-1}$ , however, provide proof of the significant  $\alpha$ -phase concentration [38]. The calculated crystal structure  $\beta$ -phases content was 81.5%, 82.8%, 85.0%, and 84.2% for PVDF and PVDF/ $\text{Co}_x\text{Zn}_{1-x}\text{Fe}_2\text{O}_4$  nanocomposite films ( $x = 0, 0.5, 1$ ), respectively. This shows that the nanofillers improved the percentage of  $\beta$ -phase in the nanocomposite films to more than 80%. This result is because the interaction between the

**Fig. 3** HRTEM and SAED of  $\text{Co}_x\text{Zn}_{1-x}\text{Fe}_2\text{O}_4$  ( $x = 0, 0.5, 1$ )

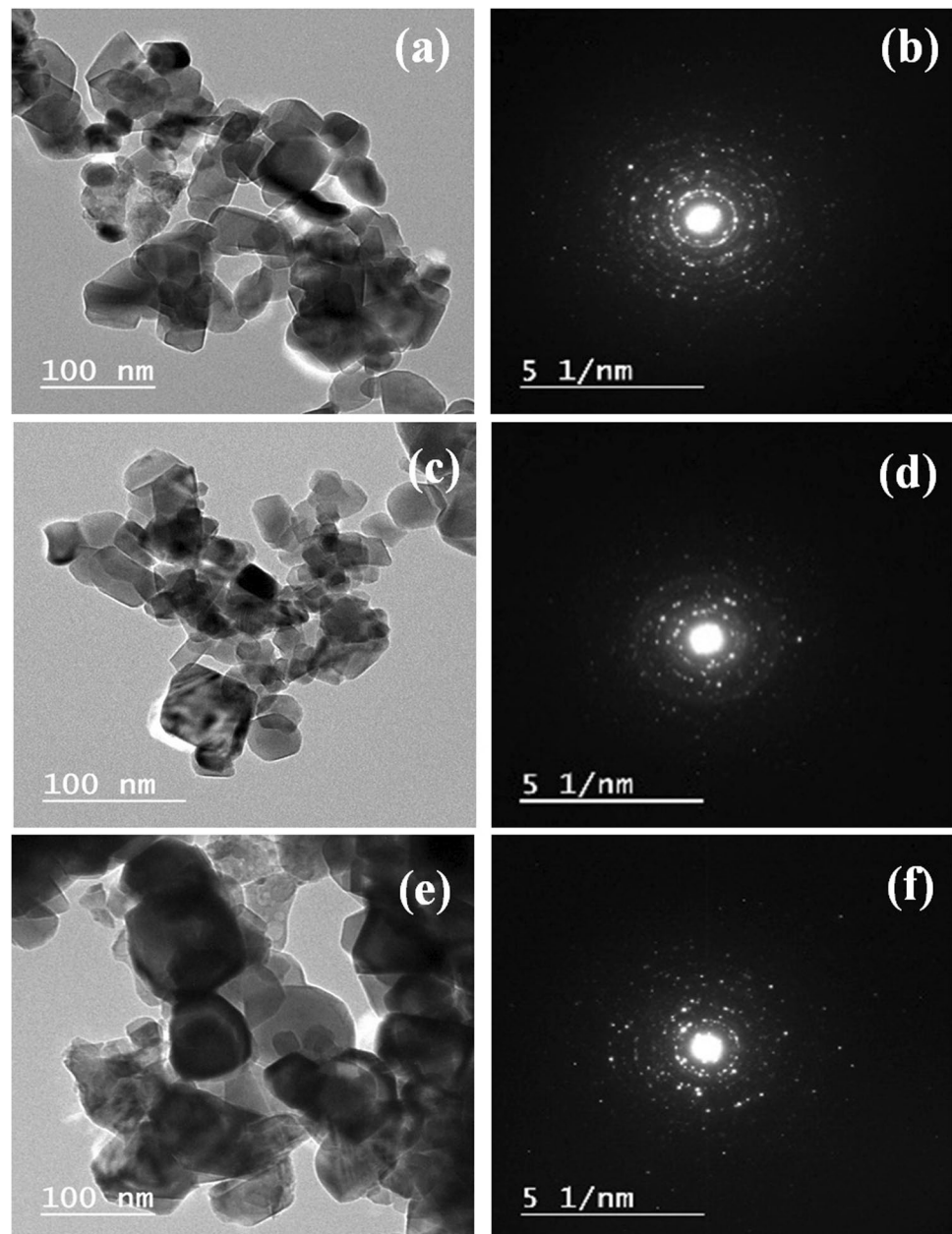
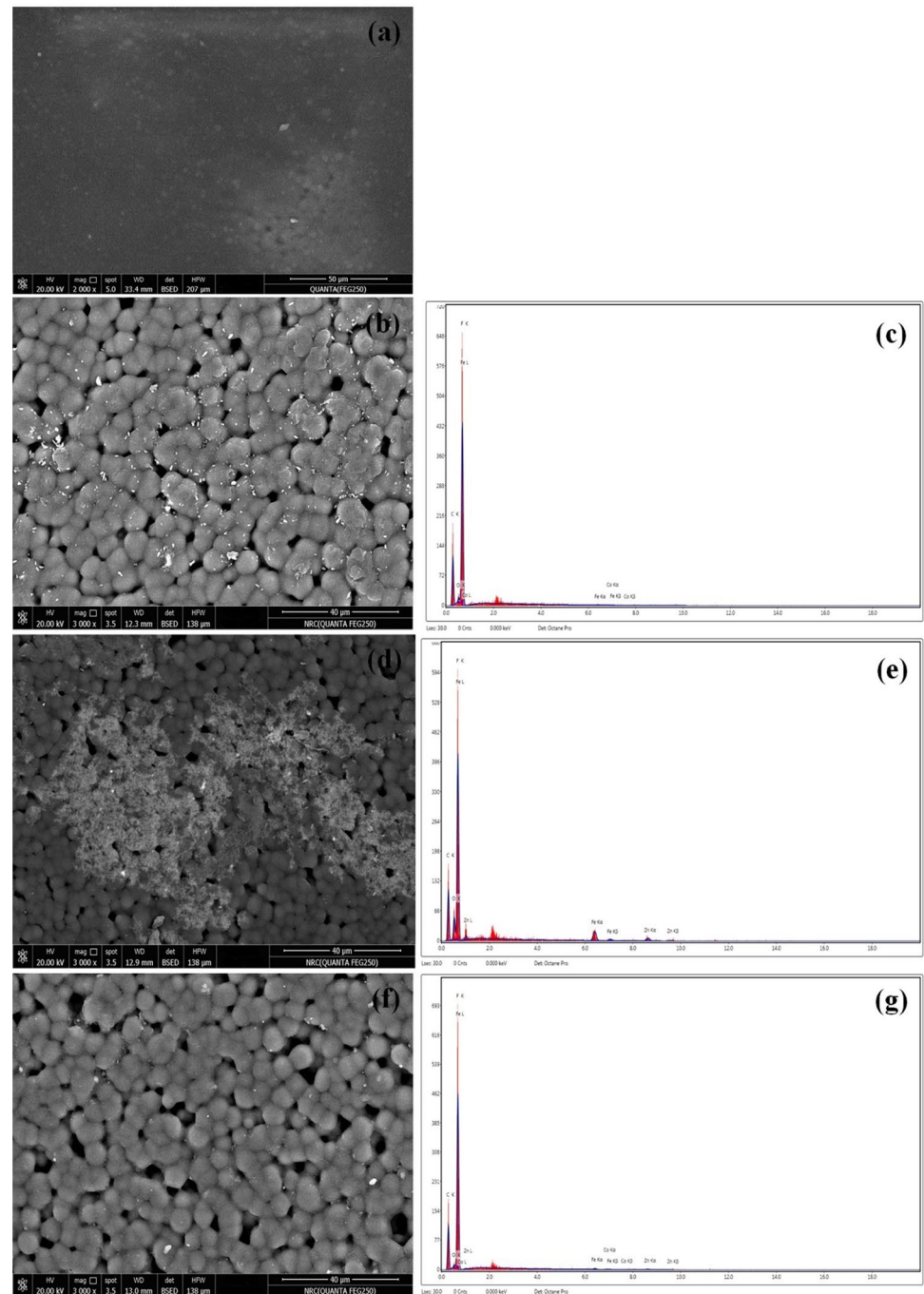


**Fig. 4** FESEM of PVDF and PVDF/ $\text{Co}_x\text{Zn}_{1-x}\text{Fe}_2\text{O}_4$  nano-composite films ( $x = 0, 0.5, 1$ )



incorporated nanoparticles and the fluorine atoms integrated into the PVDF chain structure.

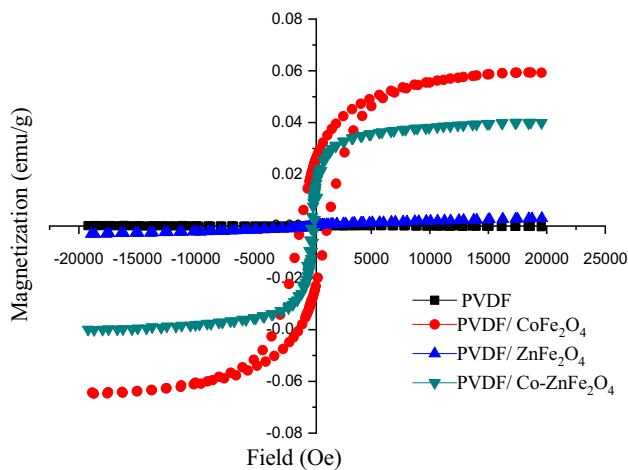
### HRTEM

Figure 3 represents the HRTEM of  $\text{CoFe}_2\text{O}_4$ ,  $\text{ZnFe}_2\text{O}_4$ , and  $\text{Co}_{0.5}\text{Zn}_{0.5}\text{Fe}_2\text{O}_4$  nanoparticles. It shows that all powders have a cubic-like shape. The size of  $\text{Co}_{0.5}\text{Zn}_{0.5}\text{Fe}_2\text{O}_4$  nanoparticles shows the largest size with average particle size 24–75 nm. The SAED image of the prepared samples confirmed the

single structure and the high crystalline nature of the prepared nanosamples which agrees with the XRD pattern.

### FESEM

Figure 4 demonstrates FESEM images of PVDF and PVDF/ $\text{Co}_x\text{Zn}_{1-x}\text{Fe}_2\text{O}_4$  nano-composite films ( $x = 0, 0.5, 1$ ). PVDF image (Fig. 4a) shows smooth and homogeneous surface. After doping, (Fig. 4b, f), the surface appeared soft, and the agglomerates particles attached to each other owing to the high magnetic



**Fig. 5** Magnetic hysteresis (M-H) loops of PVDF/M- ferrites nanocomposite films (M:  $\text{CoFe}_2\text{O}_4$ ,  $\text{ZnFe}_2\text{O}_4$ ,  $\text{Co}_{0.5}\text{Zn}_{0.5}\text{Fe}_2\text{O}_4$ )

properties of the prepared samples. It should be an advantage when these materials are investigating for specific applications such as the oil absorption capacity and heavy metal removal from aqueous solution, as the sorbent material may be easily recovered from water by using an external magnetic field [33]. It can be observed that the porosity increases with doping  $\text{Co-ZnFe}_2\text{O}_4$ . Figure 4d shows an inhomogeneous distribution of the nanoparticles in the sample included  $\text{Co}_{0.5}\text{Zn}_{0.5}\text{Fe}_2\text{O}_4$ , and this could be due to the interaction between zinc and cobalt ferrites with the PVDF chain, which make the homogeneity is an important parameter to estimate the prepared nanocomposite film properties. Also, EDX analysis confirmed the presence of nanoferrites in PVDF.

#### VSM

Figure 5 illustrates the magnetic characteristics that are shown by PVDF/Co-Zn ferrite films. These characteristics in ferrites nanopowder are highly dependent on the cation distribution, porosity, crystalline structure, grain size, grain boundary structure chemical composition, and crystal structure. However, it is possible to manipulate all these aspects of the material using appropriate synthesis techniques. The magnetic parameters that were determined based on the hysteresis loops (M-H) of each of the produced samples are listed in Table 2. The magnetic properties of PVDF/M- ferrites' nanocomposite films (M:  $\text{CoFe}_2\text{O}_4$ ,  $\text{ZnFe}_2\text{O}_4$ ,  $\text{Co}_{0.5}\text{Zn}_{0.5}\text{Fe}_2\text{O}_4$ ); films are studied through M-H plot (Fig. 5). PVDF has non-magnetic nature, and this appears, compared to the pure nanoparticles, that the value of the magnetic parameters of nanocomposites is lower [34]. Though the ferromagnetic behavior of  $\text{CoFe}_2\text{O}_4$  enhances the magnetic response of PVDF as it is clear from Table 2, a narrow loop of PVDF/ $\text{ZnFe}_2\text{O}_4$  and PVDF/ $\text{Co-ZnFe}_2\text{O}_4$  is shown in Fig. 5. The values of coercivity ( $H_c$ ) and retentivity ( $M_r$ ) as listed in Table 2 prove the antiferromagnetic nature of PVDF/ $\text{ZnFe}_2\text{O}_4$  film. We concluded that the

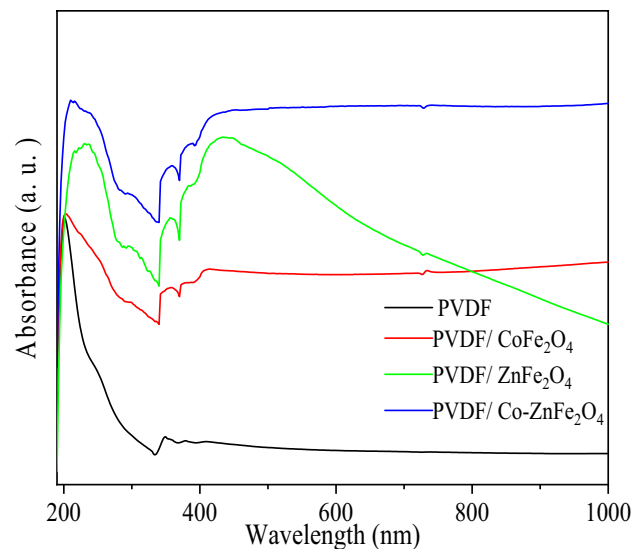


**Fig. 6** UV-Vis of PVDF and PVDF/ $\text{Co}_x\text{Zn}_{1-x}\text{Fe}_2\text{O}_4$  nanocomposite films ( $x = 0, 0.5, 1$ )

changing in magnetic parameters value by changing the nanofiller type is related to the coating of non-magnetic polymers PVDF onto nanomaterials' surface, restricting the surface defects such as pores and cracks associated with nanoferrites.

The results attained were in excellent agreement with those reported in previous studies [3–5] and support the beneficial impact of magnetic nanofillers on PVDF polymer.

#### Optical properties

Figure 6 investigates the UV-Vis spectra of PVDF and PVDF/ $\text{Co}_x\text{Zn}_{1-x}\text{Fe}_2\text{O}_4$  nanocomposite films ( $x = 0, 0.5, 1$ ). As seen PVDF has an absorption peak at 199 nm. This peak is assigned to the chromophoric group of PVDF and

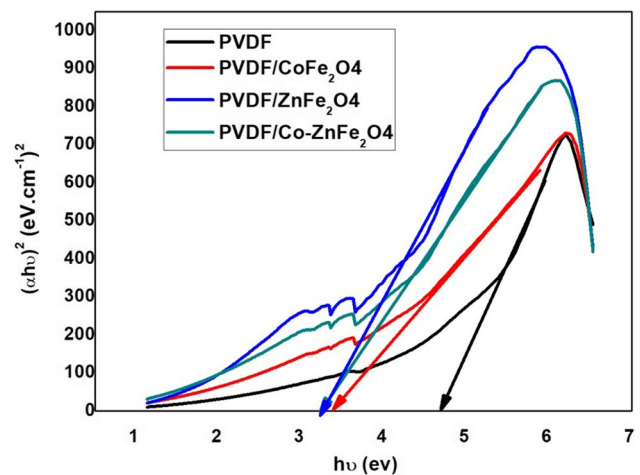


**Fig. 7** The variation of  $(\alpha h\nu)^2$  and  $h\nu$  of prepared samples

**Table 2** Magnetic parameters, including saturation magnetization ( $M_s$ ), coercive field ( $H_c$ ), a ratio of the remnant magnetization to saturation magnetization ( $M_r/M_s$ ), the hysteresis loop area for PVDF/M- ferrites nanocomposite films (M: CoFe<sub>2</sub>O<sub>4</sub>, ZnFe<sub>2</sub>O<sub>4</sub>, Co<sub>0.5</sub>Zn<sub>0.5</sub>Fe<sub>2</sub>O<sub>4</sub>)

| Composition   | $M_s$ emu/g            | $M_r^{(+)}$ emu/g     | $M_r/M_s \times 10^{-3}$ | $H_c$ (Oe) | Area erg/g $\times 10^3$ |
|---|------------------------|-----------------------|--------------------------|------------|--------------------------|
| PVDF  | $269.3 \times 10^{-6}$ | $5.4 \times 10^{-6}$  | $20.0 \times 10^{-3}$    | 4759.3     | 0.32                     |
| PVDF/CoFe <sub>2</sub> O <sub>4</sub>                                   | $62.0 \times 10^{-3}$  | $24.9 \times 10^{-3}$ | 0.4                      | 1145.3     | 229.9                    |
| PVDF/ZnFe <sub>2</sub> O <sub>4</sub>                                   | $3.1 \times 10^{-3}$   | $87.6 \times 10^{-6}$ | $28.5 \times 10^{-3}$    | 75.3       | 1.25                     |
| PVDF/Co <sub>0.5</sub> Zn <sub>0.5</sub> Fe <sub>2</sub> O <sub>4</sub> | $40.0 \times 10^{-3}$  | $6.3 \times 10^{-3}$  | 0.16                     | 115.7      | 15.9                     |

related to  $\pi$ - $\pi^*$  optical transition. After doping PVDF with metal ferrites, this peak shifted toward a higher wavelength. This red shift is due to the closer packing or agglomeration of the nanoparticles in the polymer. Also, the peak broadening increases with doping. The extremely high absorbance in the UV region related to the considered films makes it of interest in applications of UV protection. This observation confirmed the complexation between PVDF and nanoferrites. The highest absorbance intensity was observed in the PVDF/Co<sub>0.5</sub>Zn<sub>0.5</sub>Fe<sub>2</sub>O<sub>4</sub> nanocomposite film sample, which was ascribed to an increase in charge carrier concentration caused by the larger defect ratio formed by the integration of Zn and Co ferrites [39].

As is common knowledge, the analysis of the fundamental absorption edge yields important information regarding the optical band gap. An absorption edge is created when a photon excites an electron during the absorption process, moving it from a lower to a higher energy state. The optical band gap energy ( $E_g$ ) is estimated from the following relation [35]:

$$(\alpha hv) = B (hv - E_g)^{1/2} \quad (6)$$

where  $\alpha$  is the absorption coefficient and equals  $2.303(\text{absorbance})/(\text{thickness of the film})$ ,  $B$  is constant, and  $hv$  is the photon energy. Figure 7 represents the relation between  $(\alpha hv)^2$  against photon energy  $hv$ . The band gap energy is estimated from the intercept of the linear portion of the curve with zero  $hv$  axis. As observed, PVDF/Co-ZnFe<sub>2</sub>O<sub>4</sub> nanoparticles have the lowest band gap energy which makes it useful for photocatalytic and electrical application. This is because the number of final states in the system changes because of the development of new localized states in the band gap and the increase of the charge carrier's concentration due to defects [39].

## Conclusion

Nanoferrite fillers with different compositions of CoFe<sub>2</sub>O<sub>4</sub>, ZnFe<sub>2</sub>O<sub>4</sub>, and Co-ZnFe<sub>2</sub>O<sub>4</sub> were prepared successfully by using citrate auto-combustion method. Then, these nanofillers were included to PVDF polymers to make nanocomposite films of PVDF/(CoFe<sub>2</sub>O<sub>4</sub>, ZnFe<sub>2</sub>O<sub>4</sub>, and Co-ZnFe<sub>2</sub>O<sub>4</sub>). The structure of the prepared nanocomposites film was studied using XRD and FTIR. It is observed in HRTEM that the particle size obtained

from the HRTEM is larger than that obtained from XRD owing to the agglomeration and formation of nanoclusters. This agglomeration could be related to the high magnetic response of the prepared nanofiller. FESEM demonstrated that the insertion of nanoferrites into PVDF polymers generates pores and that the addition of PVDF/Co-ZnFe<sub>2</sub>O<sub>4</sub> increases the pore size of the PVDF surface. Consequently, adding these nanofillers to PVDF, causing enhancement of the magnetic properties of the PVDF, and making these films to be suitable for different applications. PVDF/Co-ZnFe<sub>2</sub>O<sub>4</sub> has the smallest band gap energy, according to calculations, making it applicable in photochemical and electrical situations.

**Funding** Open access funding provided by The Science, Technology & Innovation Funding Authority (STDF) in cooperation with The Egyptian Knowledge Bank (EKB).

## Declarations

**Conflict of interest** The authors declare no competing interests.

**Open Access** This article is licensed under a Creative Commons Attribution 4.0 International License, which permits use, sharing, adaptation, distribution and reproduction in any medium or format, as long as you give appropriate credit to the original author(s) and the source, provide a link to the Creative Commons licence, and indicate if changes were made. The images or other third party material in this article are included in the article's Creative Commons licence, unless indicated otherwise in a credit line to the material. If material is not included in the article's Creative Commons licence and your intended use is not permitted by statutory regulation or exceeds the permitted use, you will need to obtain permission directly from the copyright holder. To view a copy of this licence, visit <http://creativecommons.org/licenses/by/4.0/>.

## References

1. Ramadan, R., Ismail, A.M.: Tuning the physical properties of PVDF/PVC/zinc ferrite nanocomposites films for more efficient adsorption of Cd (II). *Journal of Inorganic and Organometallic Polymers and Materials*. **32**(3), 984–998 (2022)
2. Etemadi, H., Afsharkia, S., Zinatloo-Ajabshir, S., Shokri, E.: Effect of alumina nanoparticles on the antifouling properties of polycarbonate-polyurethane blend ultrafiltration membrane for water treatment. *Polymer Engineering & Science*. **61**(9), 2364–2375 (2021)
3. Zinatloo-Ajabshir, S., Heidari-Asil, S.A., Salavati-Niasari, M.: Simple and eco-friendly synthesis of recoverable zinc cobalt oxide-based ceramic nanostructure as high-performance photocatalyst for enhanced photocatalytic removal of organic contamination under solar light. *Separation and Purification Technology*. **267**, 118667 (2021)



4. Soltaninejad, V., Ahghari, M.R., Taheri-Ledari, R., Maleki, A.: Bifunctional PVA/ZnO/AgI/chlorophyll nanocomposite film: enhanced photocatalytic activity for degradation of pollutants and antimicrobial property under visible-light irradiation. *Langmuir*. **37**(15), 4700–4713 (2021)
5. Rahimi, J., Taheri-Ledari, R., Niksefat, M., Maleki, A.: Enhanced reduction of nitrobenzene derivatives: effective strategy executed by Fe<sub>3</sub>O<sub>4</sub>/PVA-10% Ag as a versatile hybrid nanocatalyst. *Catalysis Communications*. **134**, 105850 (2020)
6. Osman, C.B., Nowak, S., Garcia-Sanchez, A., Charles, Y., Ammar, S., Mercone, S., Mammeri, F.: In situ monitored stretching induced  $\alpha$  to  $\beta$  allotropic transformation of flexible poly (vinylidene fluoride)-CoFe<sub>2</sub>O<sub>4</sub> hybrid films: the role of nanoparticles inclusion. *European Polymer Journal*. **84**, 602–611 (2016)
7. Choi, M.H., Yang, S.C.: CoFe<sub>2</sub>O<sub>4</sub> nanofiller effect on  $\beta$ -phase formation of PVDF matrix for polymer-based magnetoelectric composites. *Materials Letters*. **223**, 73–77 (2018)
8. El-Masry, M.M., Ramadan, R.: The effect of CoFe<sub>2</sub>O<sub>4</sub>, CuFe<sub>2</sub>O<sub>4</sub> and Cu/CoFe<sub>2</sub>O<sub>4</sub> nanoparticles on the optical properties and piezoelectric response of the PVDF polymer. *Applied Physics A*. **128**(2), 1–13 (2022)
9. Kaur, G.A., Pratiksha, M.S., Kumar, S.: Ferroelectrics Letters Section. **49**, 51 (2022)
10. Guleria, G., Thakur, S., Sharma, D.K., Thakur, S., Kumari, P., Shandilya, M.: Advances in natural sciences: nanoscience and nanotechnology. **13**, 025004 (2022)
11. Haponska, M., Trojanowska, A., Nogalska, A., Jastrzab, R., Gumi, T., Tylkowski, B.: PVDF membrane morphology—influence of polymer molecular weight and preparation temperature. *Polymers*. **9**(12), 718 (2017)
12. Miranda, M.A.R., Sasaki, J.M.: The limit of application of the Scherrer equation. *Acta Crystallographica Section A: Foundations and Advances*. **74**(1), 54–65 (2018)
13. Ramadan, R.: Physical study of cobalt ferrite and its application in purification of water. *Applied Physics A*. **125**(12), 1–8 (2019)
14. Singh, N.B., Rachna, K.: Copper ferrite-polyaniline nanocomposite and its application for Cr (VI) ion removal from aqueous solution. *Environmental nanotechnology, monitoring & management*. **14**, 100301 (2020)
15. Al Kiey, S.A., Ramadan, R., El-Masry, M.M.: Synthesis and characterization of mixed ternary transition metal ferrite nanoparticles comprising cobalt, copper and binary cobalt–copper for high-performance supercapacitor applications. *Applied Physics A*. **128**(6), 1–13 (2022)
16. Cheng, Y., Li, Z., Li, Y., Dai, S., Ji, G., Zhao, H., Du, Y.: Rationally regulating complex dielectric parameters of mesoporous carbon hollow spheres to carry out efficient microwave absorption. *Carbon*. **127**, 643–652 (2018)
17. You, H., Zhang, L., Jiang, Y., Shao, T., Li, M., Gong, J.: Bubble-supported engineering of hierarchical CuCo<sub>2</sub>S<sub>4</sub> hollow spheres for enhanced electrochemical performance. *Journal of Materials Chemistry A*. **6**(13), 5265–5270 (2018)
18. Kaur, G.A., Shandilya, M., Rana, P., Thakur, S., Uniyal, P.: Nanostructures and nano-objects. **22**, (2020)
19. Sharma, S., Shandilya, M., Rai, R.: *Journal of Materials Science: Materials in Electronics*. **26**, (2015)
20. Shandilya, M., Verma, R.: *Journal of Magnetism and Magnetic Materials*. **527**, (2021)
21. Shandilya, M., Thakur, S., Thakur, S.: *Cellulose*. **27**, (2020)
22. El-Masry, M.M., Ramadan, R.: *Journal of Materials Science: Materials in Electronics*. **33**, 15946 (2022)
23. El-Masry, M.M., Ramadan, R.: *Applied Physics A - Materials Science & Processing*. **128**, (2022)
24. El-Masry, M.M., Ibrahim, A.S.: *Journal of Materials Science: Materials in Electronics*. **33**, (2022)
25. Patterson, A.L.: The Scherrer formula for X-ray particle size determination. *Physical Review*. **56**(10), 978 (1939)
26. Chen, N., Pan, Q.M.: Versatile fabrication of ultralight magnetic foams and application for oil-water separation. *ACS Nano*. **7**(8), 6875–6883 (2013)
27. Liu, Q., Zhong, L.B., Zhao, Q.B., Frear, C., Zheng, Y.M.: Synthesis of Fe<sub>3</sub>O<sub>4</sub>/polyacrylonitrile composite electrospun nanofiber mat for effective adsorption of tetracycline. *ACS Applied Materials & Interfaces*. **7**(27), 14573–14583 (2015)
28. Kumar, D., Kumar, S., Kumar, S., Thakur, N., Shandilya, M.: *Physica Status Solidi (a)*. **2200238**, (2022)
29. G. Rana, G. A. Kaur, S. Thakur, and M. Shandilya, (2022), p. 050002.
30. El-Masry, M.M., Ramadan, R., Ahmed, M.K.: The effect of adding cobalt ferrite nanoparticles on the mechanical properties of epoxy resin. *Results in Materials*. **8**, 100160 (2020)
31. Dabas, S., Chahar, M., Thakur, O.P.: Electromagnetic interference shielding properties of CoFe<sub>2</sub>O<sub>4</sub>/polyaniline/poly (vinylidene fluoride) nanocomposites. *Materials Chemistry and Physics*. **278**, 125579 (2022)
32. Schulz, R.B., Plantz, V.C., Brush, D.R.: Shielding theory and practice. *IEEE Transactions on Electromagnetic Compatibility*. **30**(3), 187–201 (1988)
33. Kumar, S., Verma, V., Walia, R.: Magnetization and thickness dependent microwave attenuation behavior of Ferrite-PANI composites and embedded composite-fabrics prepared by in situ polymerization. *AIP Advances*. **11**(1), 015106 (2021)
34. Stejskal, J., Gilbert, R.G.: Polyaniline. Preparation of a conducting polymer (IUPAC technical report). *Pure and applied chemistry*. **74**(5), 857–867 (2002)
35. Abdalkarim, K.A., Aziz, S.B., Abdulwahid, R.T., Alshehri, S.M., Ahamad, T., Hadi, J.M., Hussein, S.A.: Synthesis of Hg metal complex and its application to reduce the optical band gap of polymer. *Arabian Journal of Chemistry*. **14**(7), 103215 (2021)
36. Frost, R.L., Erickson, K.L., Weier, M.L., Carmody, O.: Raman and infrared spectroscopy of selected vanadates. *Spectrochimica Acta - Part A: Molecular and Biomolecular Spectroscopy*. **61**(5), (2005). <https://doi.org/10.1016/j.saa.2004.06.006>
37. Petrovskii, S.K., Stepanova, O.G., Vorobyeva, S.S., Pogodaeva, T., v., & Fedotov, A. P.: The use of FTIR methods for rapid determination of contents of mineral and biogenic components in lake bottom sediments, based on studying of East Siberian lakes. *Environmental Earth Sciences*. **75**(3), (2016). <https://doi.org/10.1007/s12665-015-4953-y>
38. Shepelin, N.A., Glushenkov, A.M., Lussini, V.C., Fox, P.J., Dicinowski, G.W., Shapter, J.G., Ellis, A.V.: *Energy. Environmental Science*. **12**, (2019)
39. Pandey, S., Pandey, S.K., Parashar, V., Mehrotra, G.K., Pandey, A.C.: *Journal of Materials Chemistry*. **21**, (2011)

**Publisher's note** Springer Nature remains neutral with regard to jurisdictional claims in published maps and institutional affiliations.